# Structural Analysis of a Stress-Laminated-Timber Bridge Deck Using Hardwood

Marcio Lima do Nascimento, Ph.D.[1]; Edson Fernando Castanheira Rodrigues, P.G.[2]; André Luis Christoforo, Ph.D.[2]; Francisco Antonio Rocco Lahr, Ph.D.[3]; and Giovana Gobatto Balanco, P.G.[4]

**Abstract:** The abundance of wood in Brazil combined with the advantages of its use has lead to many studies focusing on optimizing the application of this raw material. In particular, stress-laminated-timber decks are an alternative to conventional building materials for short- to medium-span bridges, and its advantages include low weight and excellent flexibility that enable a high prefabrication rate and quick assembly on site. In order to make the best use of wood, this work studies the behavior of a stress-laminated-timber bridge deck using hardwoods. In brief, three different species were used as laminates, which with the prestress effect made it really difficult to have optimal precision in the numerical analysis, then resulting in higher displacements than those from the tests in almost all comparisons. However, the results of the experimental and numerical displacements followed the same pattern and linearity with reasonable values and low deflections, which demonstrates that the system worked as an orthotropic plate equivalent to the same deck system constructed out of conifers, as widely used in North America for such structures. Further research should be performed with one species only, so that even better results could be found.
**DOI: 10.1061/(ASCE)BE.1943-5592.0001658**. 



## Introduction

Brazil is one of the leading countries in the world in terms of the forest sector, as it has a certified forest area of 6,378,006 ha in different biomes, each with specific flora characteristics (Cavalheiro et al. 2018). Physical and mechanical characteristics and relative abundance of this material enable its application from interiors and furniture to roofs, bridges, and high-rise buildings. Moreover, wood has environmental advantages when compared with other building materials (e.g., cement, concrete, steel and aluminum) because it is recyclable, renewable, biodegradable, and requires low energy for processing (Marques 2008; Aydemir et al. 2015; Segundinho et al. 2018; Rodrigues and Christoforo 2019).

Regarding the importance of wood and all the advantages involved, such material is commonly used in the construction and design of bridges of many structural systems, such as the deck of the stress-laminated-timber (SLT) bridges, which have been studied by authors around the world. It may be tempting to think that SLT decks are not ideal from the point of view of rational use of wood, but there are several important advantages to such type of bridge deck, including low weight, simplicity and high speed of manufacture, ease of transport, quick assembly, and excellent adaptability/flexibility to complicated geometries even with the horizontal curvature of the roadway. As a result of such qualities, SLT decks ensure low cost and great performance, which makes them a good alternative to conventional building materials for short- to medium-span bridges (Crocetti et al. 2015; Ekholm and Kliger 2014).

The SLT assembly is composed of timber laminations placed side by side, which are compressed perpendicular to the grain by prestressed high-strength steel bars. As a result of the prestress, a resisting frictional force between the timber laminations produces a plate that exhibits orthotropic behavior. In addition, this behavior has been described by several authors (Bakht and Jaeger 1985; Oliva and Dimakis 1988; Ritter 1990; Ritter et al. 1990; Davalos et al. 1996; Stavridis 2001; Crews 2002; Karlsson et al. 2009; Ekevad et al. 2011; Ekholm et al. 2012, 2013; Ekholm and Kliger 2014; Crocetti et al. 2015), and in all the cases, the decks were constructed out of timber laminations extracted from coniferous tree species. Bakht and Jaeger (1985) developed a simplified analysis of the orthotropic method using conifer species (particularizing the case of SLT bridges) that was based on two distribution coefficients, the torsional parameter ($\alpha$) and flexural parameter ($\theta$), which characterize the deflections of orthotropic rectangular plates. According to Williamson (1990), it was also observed that for bridges built in the US, with deflection up to 1/400 L considering live load for HS20-44 (324 kN), there was no problem of slow post-deformation, although Ritter et al. (1990) found out that some SLT decks assembled from green wood (conifer species), monitored in the US, exhibited a loss of prestress of 80% in 2 years. A possible solution introduced by Crocetti et al. (2015) is the use of screws as local reinforcement for high compression perpendicular to the grain, therefore reducing the loss of prestressing force in the prestressing bars.

Regarding not only deformation, but the vibration of bridges, Schubert et al. (2010) developed an experimental and computational (finite element (FE) method) analysis to measure values of vibration of two types of wood bridges, of which the deck plates were designed with cross-laminated timber (CLT) and SLT. The results pointed to a reduction of vibration and gain in stiffness of the decks when using asphalt pavement. Crocetti et al. (2015) suggested that the weakening effect of butt joints on the stiffness and strength of the SLT deck should be analyzed, as in Ekholm and Kliger (2014).

[1]Dept. of Mathematics, Federal Univ. of Pará (UFPA), Belém 66075-110, Brazil.
[2]Dept. of Civil Engineering (DECiv), Federal Univ. of São Carlos (UFSCar), São Carlos 13565-905, Brazil.
[3]Dept. of Structural Engineering (SET), São Carlos Engineering School (EESC), São Paulo Univ. (USP), São Carlos 13566-590, Brazil.
[4]Dept. of Structural Engineering (SET), São Carlos Engineering School (EESC), São Paulo Univ. (USP), São Carlos 13566-590, Brazil (corresponding author). ORCID: https://orcid.org/0000-0002-2544-3743. Email: giovanaagobatto@hotmail.com

Note. This manuscript was submitted on November 21, 2019; approved on August 27, 2020; published online on January 11, 2021. Discussion period open until June 11, 2021; separate discussions must be submitted for individual papers. This paper is part of the ***Journal of Bridge Engineering***, © ASCE, ISSN 1084-0702.

The main objective of Crocetti et al. (2015) was to evaluate the state of the art and design based on the Swedish practice of SLT decks with Glulam beams of strength class of GL28c. The authors also showed that the span had no influence on the longitudinal bending moment or transverse and longitudinal shear forces, and highlighted the best practices regarding some detailing, water protection, and durability of a SLT deck. Ekholm and Kliger (2014) studied the effect of interlaminar slip and butt joints in a narrow SLT bridge deck assembled of Norway spruce (*Picea abies*), a conifer species. There were six high-strength steel bars for prestressing used through the SLT bridge deck, and the variables analyzed were the height of laminates and the width, prestress level, position and intensity of applied load, parallel and perpendicular coefficient of friction (COF), and the number and positions of butt joints. Thus, with these variables, the comparison of load deflection was analyzed from both experimental tests and the numerical analyses in order to improve the accuracy of the numerical model.

Still trying to improve knowledge of the mechanical behavior of SLT decks, Ekholm et al. (2012) confronted the literature and some standards regarding the linearity until failure in the structural response of a SLT bridge deck using a softwood species (Norway spruce, *P. abies*) as the laminate. Nondestructive and destructive tests were performed on a SLT deck with a span of 4.9 m and thickness of 270 mm. A full-scale test of the SLT deck was performed to obtain the deformations at various prestress levels as well as the ultimate load capacity of such a structure with loads applied as a single axle positioned centrically and eccentrically on the plate. As a result, the deflections found were 10% larger at a prestress level of 300 kN compared with prestress levels of 600 and 900 kPa, and, lastly, the failure occurred with an eccentric loading of 900 kN and an applied prestress of 600 kPa. It was also inferred that in some points of the deck, the deflection was nonlinear, which the authors suggested that could be caused by interlaminar slip between the laminates, so that the linearity seems to be dependent on the applied prestress intensity.

Concerning the rheological and thermohygromechanical behavior of a SLT deck under variable environmental conditions (variation of temperature and relative humidity), Figueroa et al. (2012) performed a study of a SLT deck constructed out of the softwood species *Pino radiate*. The authors applied four types of preservative treatment to the samples, which were subjected to four cycles of temperature and relative humidity in a climate chamber, with a total of 16 specimens. As a consequence, a significant stress reduction in the steel bars during a condition representing the summer season and a significant increase of stress during the winter were verified, and significant differences of deformation behavior between untreated and treated (with preservatives) samples were observed in each cycle. However, there was no evidence of thermohygromechanical fluency or wood relaxation under the conditions considered in the study. Ekholm et al. (2013) compared several linear design methods with each another and with an ultimate load test of a full-scale SLT deck subjected to an eccentric load. The deck was made out of Glulam beams of Norway spruce (*P. abies*). All design methods failed to predict deflections of the tested deck when loaded to failure owing to the nonlinear behavior in this situation, which was also confirmed by Ekholm et al. (2012). The apparent modulus of elasticity (MOE) was found to have the greatest influence on overall stiffness of the deck. When compared, neither the Ritter or Crews equivalent beam theory was suitable when the load was positioned at the very edge of the deck. The equivalent beam method in CEN (2004) was very conservative and it gave values that were too large for deflection when applying centric loading. However, the same method produced reasonable results when an eccentric load was positioned at the very edge of the plate.

The behavior of a SLT deck made of conifer species has been the target of several studies in North America. The use of hardwood in this system could lead to results far different from those found with softwood owing to the transverse stiffness caused by prestress and the torsional stiffness.

The aim of this paper was to validate a SLT bridge deck assembled with hardwood by comparing results from both experimental and FE analysis using an orthotropic plate method adopted from Ritter (1990) to calculate the same type of bridge normally assembled from conifers. The main properties analyzed were the transverse stiffness caused by prestress and the torsional stiffness.

## Materials and Method

A SLT deck bridge made entirely out of hardwood was tested so that a compatible model could be validated by means of SAP 90, through a FE analysis. The analogy adopted to determine the carrying capacity of the SLT deck was the orthotropic plate, and such behavior must be guaranteed by the prestress implemented and maintained within an adequate level. Furthermore, an orthotropic plate has constant thickness, but with different properties of flexion and torsion in its mutually perpendicular directions, and the shear force is considered negligible in the calculation of deflections.

The simplified calculation of particularized orthotropic plate theory for the bridge in this paper was developed by Bakht and Jaeger (1985) based on the concept of characterization parameters, which defines, for example, a relation between the structural properties of two structures so that they have the same deflection pattern when subjected to the same load pattern. These can be summarized in one parameter of flexion $\theta$ and another of torsion $\alpha$. When the same load pattern is applied to rectangular plates, they are going to have the same deflection profile if these flexural and torsional parameters ($\theta$; $\alpha$) were the same for those plates. SLT bridges have been calculated by this method, which is based on the orthotropic plate theory, as mentioned previously, and can provide a faster analysis of the effort involved and minimum requirements of design.

The structure considered as the reference to the present assembly model is the White Oak Bridge, in Chattahoochee National Forest (United States), reported by Taylor and Ritter (1990), and built out of spruce in 1989, with dimensions of 9 m length, 6 m width, and 40.5 cm thickness. The idea of assembling the present model was inspired by the concept of characterization parameters, so these same parameters as in the White Oak Bridge were adopted. Although the research did not consider a prototype with the same dimensions, the same parameters used made it possible to establish a ratio between the referential model and prototype in order to evaluate the stiffness parameters and validate the theoretical model. Thus, the reduction scale adopted was 1:3.75, which means a total span of 2.40 m, free span of 2.20 m, width of 1.60 m, and thickness of 11 cm as a consequence of the size of the wooden elements and availability of experimental devices in the laboratory.

### *Bridge Model*

A SLT deck model 2.40 m long (free span of 2.20 m) and 1.62 m wide was constructed out of beams with cross-sectional area of $6 \times 11\ \text{cm}^2$, which were transversely prestressed by steel bars with 12.7 mm diameter, forming a plate 11 cm thick. Initially, 6 species were selected and tested in compression parallel to the fibers in accordance with NBR 7190 (1997), although only 3 species were chosen as their MOE values were closer to each other than the other 3 hardwood species, resulting in 27 laminates of the 3 chosen species for the construction of the SLT plate.

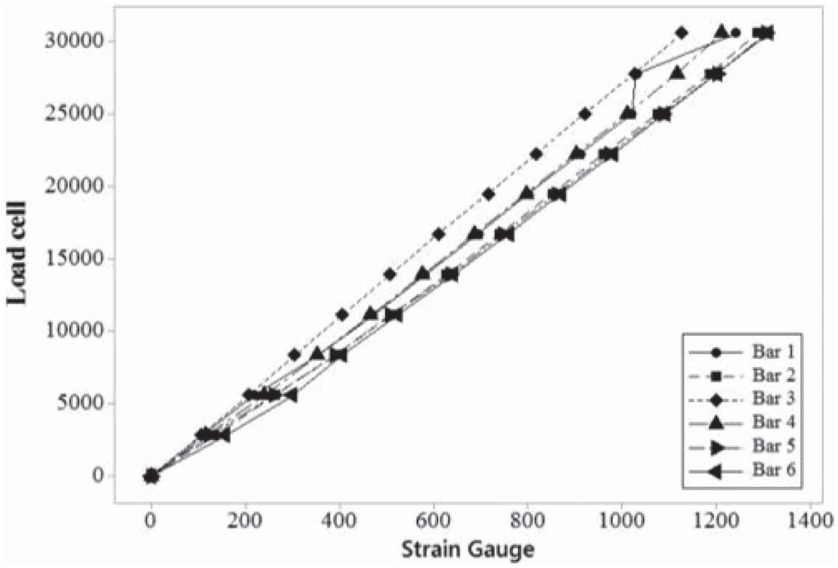


**Fig. 1.** Calibration of the bars.

The three species used were: *Cedrela odorata* (10 laminates), *Vataireopsis araroba* (7 laminates) and *Aspidosperma polyneuron* (10 laminates), which were divided into three groups: 9–11 (MOE between 9,000 and 11,000 MPa); 11–13 (between 11,000 and 13,000 MPa), and 13–15 (between 13,000 and 15,000 MPa) that correspond to *C. odorata*, *V. araroba*, and *A. polyneuron*, respectively. As a consequence of the range of species and laminates, the mean longitudinal MOE of the beams was equal to 12.309.8 MPa, with a standard deviation of 2.267 MPa (18%) and a moisture content of 12%, which was also used in the numerical analysis for the entire SLT deck.

### Board Instrumentation

The evaluation of the prestressing force into the rod was performed through electric strain gauges bonded to the bars in order to obtain the correlation between the strain measures and the applied tensile force. Thus, the calibration of strain gauges attached to the prestressing bars were performed using the following equipment: DIFASA 30 kN capacity hollow hydraulic cylinders; 50 kN load cell; electric strain gauges KFC 10/C1/11 gauge factors 2.10; KYOWA deformation indicator; and Hewlett Packard (HP) data acquisition system.

The electric strain gauges were positioned in the midlength of the bars, whereas the cylinder and the load cell were placed at the edge. When operated, the cylinder compressed the load cell that in turn pressed the anchorage plate, thus tensioning the bar. The data for this calibration are presented in Fig. 1 and linear regressions (obtained from the data contained in Fig. 1) are presented in Fig. 2 in which $Y$ is the reading of the load cell at the edge and $X$ is the reading in midspan of the bars. As a consequence of the test, it was possible to evaluate in each bar, the strain recorded in the extensometer that corresponded to a tension of 30 kN (prestressing load). Thus, the prestressing turned out to be simple as the registration was only done via the electric extensometer, although the nuts were tightened on the anchor plates manually.

Furthermore, for the measurement of specific displacements and deformations, 19 displacement transducers and 24 electric strain gauges were connected to the HP 9825T data acquisition system. The displacement transducers were used by means of the HP 24

Bar 1: $Y = 2.52545X$
Bar 2: $Y = 2.4826X$
Bar 3: $Y = 2.7148X$
Bar 4: $Y = 2.5372X$
Bar 5: $Y = 2.3621X$
Bar 6: $Y = 2.4301X$

**Fig. 2.** Linear regressions from the calibration of the bars.

DCT model with the amplitude equal to $\pm 12$ mm and precision of one-hundredth of a millimeter. As a representation of the instrumentation, Fig. 3 shows the location points on the upper and lower sides of the SLT deck plate.

### Support Setting, Framework, and Reaction Board

The reduced model was supported on a system composed of rolled steel joists, which, in turn, were supported by the reaction board. In addition, the load application was carried out with the aid of a framework also composed of I-shaped cross-section beams that were positioned over the system of support as shown in Fig. 4.

### Devices for Load Application

The loads were applied to the model by means of a hydraulic cylinder with a nominal load capacity of 150 kN, which was coupled to the I-beams and steel plates of the framework. The applied load was distributed over an area of 300 $cm^2$ through 15 cm × 20 cm steel sheet surface of 2.5 cm thickness. Moreover, there was no concern with simulating a model representing a wheel contact area of any vehicle type owing to this deck system be constituted without spars, thus making it possible to perform a simplified analysis with concentrated loads on the plate, which can provide significant data that represents its structural behavior (Bakht and Jaeger 1992).

### Assembly of the Model

Initially the prestressing bars were placed on the reaction board in the predefined positions spaced 40 cm apart. Then the predrilled beams were positioned longitudinally (perpendicular to the bars) and placed from the transversal edges to the middle of the plate,

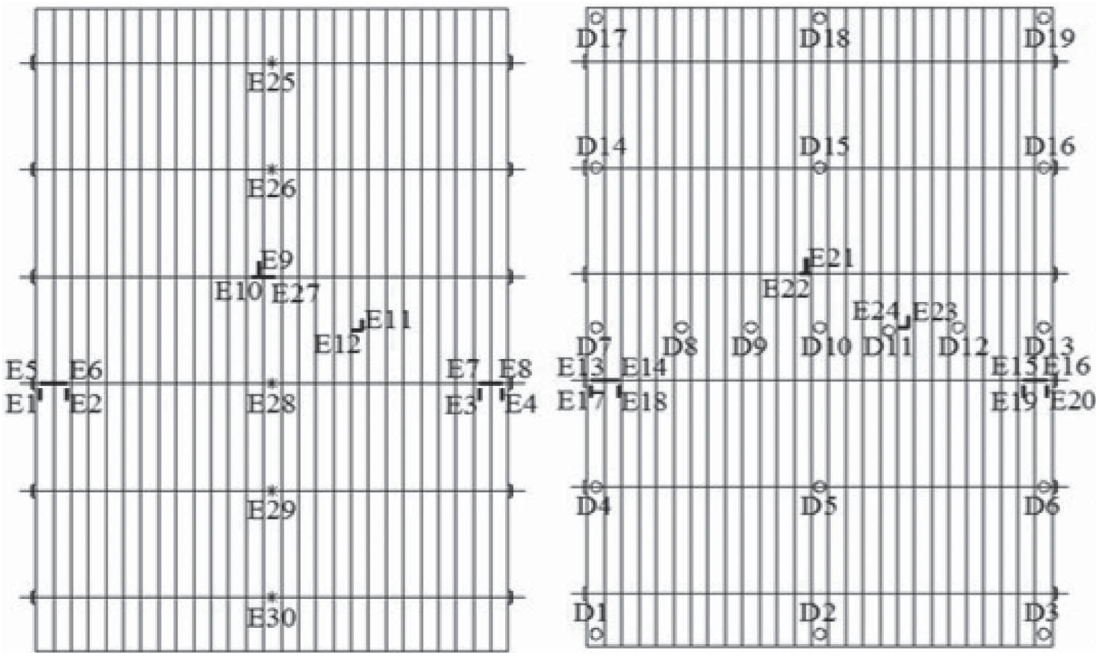


**Fig. 3.** Location and instrumentation points of (a) the upper face and (b) the lower face of the plate.

**Fig. 4.** Experimental deck and its supports. (Image by Marcio Lima do Nascimento.)

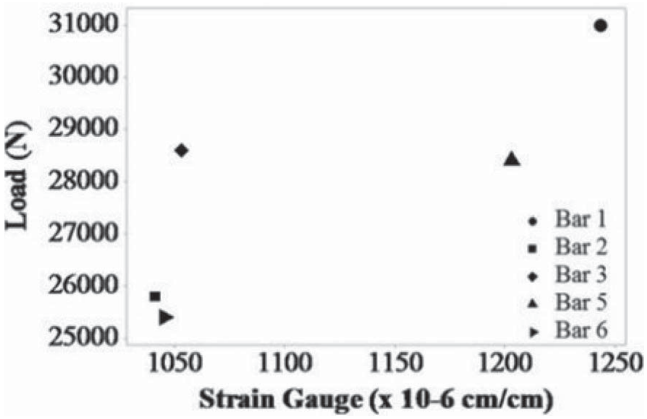


**Fig. 5.** Reading of the strain gauges in the bars after the last tightening over the nuts.

with the more stiff laminates ($E$ between 13,000 and 15,000 MPa) being positioned in the edges and in the middle of the board. Furthermore, in the two beams located in the transversal midspan of the deck, small holes were drilled so that the wiring of the extensometers connected to the steel bars could be plugged into the data acquisition system.

With the steel beams and bars in place, the anchorage system was assembled by placing the anchorage plates and nuts, and initially tightening them. Next, the SLT deck was lifted and placed in the test position on the supports so that the instrumentation phase of the plate could be started in which 24 electric strain gauges were bonded to the upper and lower sides of the beams and 19 linear variable differential transformers (LVDTs) were positioned under the plate as can be seen in Fig. 3. Therefore, once the SLT plate was assembled and instrumented, it was possible to perform the prestress and subsequent load tests on the deck.

### *Prestressing and Anchorage System of the Model*

The prestressing system consisted of 6 steel bars spaced 400 mm from each other and, for each bar, the prestressing load calculated as a function of the minimum interlaminar compression required on the Ontario Highway Bridge Design Code resulted in

$$F = 700\,\text{kN/m}^2 \times 0.40\,\text{m} \times 0.11\,\text{m} = 30.8\,\text{kN (prestressing load)}$$

Thus, it was possible to manually implement this prestressing load in the bars as a consequence of the relatively low calculated value (30.8 kN), whereas the main concern during the manual prestress was to avoid the rotation of the steel bars, which could result in eventual damage to the strain gauges, thereby compromising the readings. Thus, carefully, the final tensile loads after the last tightening were recorded and displayed in Fig. 5.

Moreover, Fig. 5 does not show any value for extensometer 4 that was discarded after the fourth tightening of the nuts caused by a reading malfunction. Thus, although the last reliable reading

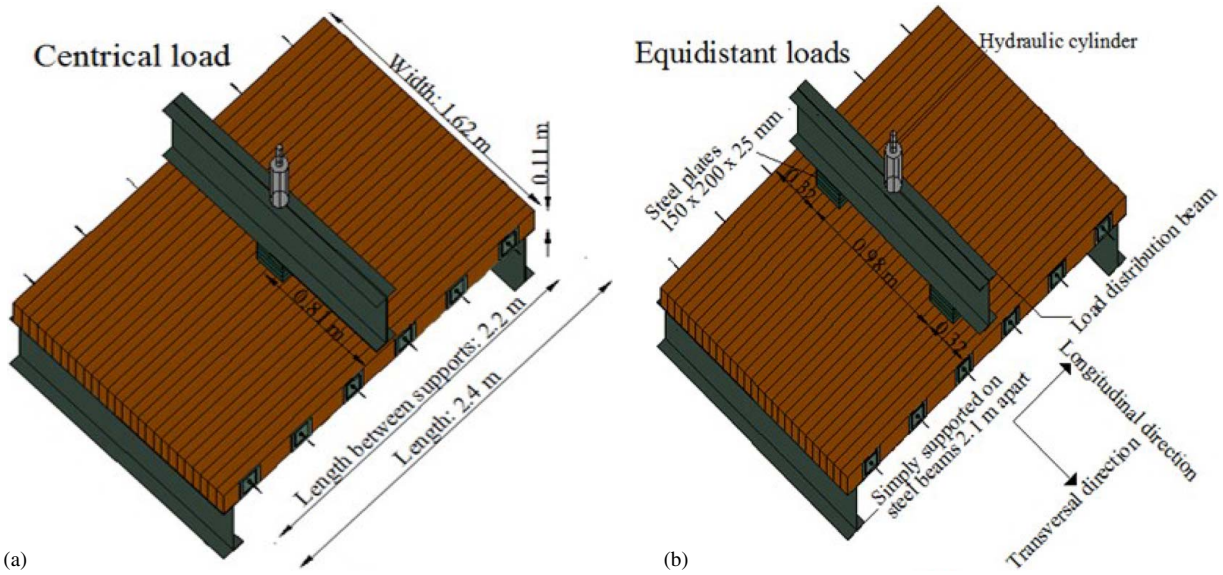


**Fig. 6.** Configuration of the laminated prestressed plate tested with the support condition, plate measurements, and position of the test load in (a) test 1 plus the directions of the deck and position of the loads in (b) test 2.

recorded was $973 \times 10^{-6}$ cm/cm (third reading), in the remainder of the test it was not possible to evaluate the tensile strength in this bar.

As high-strength steel bars are used as reinforcement in full-scale bridges, CA-32 ($F_{yk} = 320$ MPa) structural steel with a diameter of 12.7 mm was used owing to the availability of materials in the laboratory. After choosing the steel type, tensile tests were performed on this structural steel that resulted in a yield load of 42.5 kN. Furthermore, the discrete plate system was used to anchor the bars to the laminates, as widely implemented in the United States, and in this particular study was constituted by two steel plates of the following dimensions:

- smaller steel plate = 10 cm × 8 cm; and
- larger steel plate = 15 cm × 10 cm.

The prestress performed manually provided conditions to obtain an approximate prestressing load of 28 kN that was close to the intended value (30.8 kN traction). However, the application of prestress through hydraulic cylinders could lead to more satisfactory and accurate results. In addition, the evaluation of the prestressing load through the reading of electrical strain gauges did not present the expected efficiency, precisely because of the problems with manual tightening.

In addition to being careful not to break the strain gauges, it was difficult to evaluate the behavior of the prestressing load over time, because the program that converted the voltage read from the strain gauges into deformation measures was not able to take the readings after the prestress process, because the reading always started from a zero strain mark after each tightening. The most viable alternative would be the use of load cells in one or two rods for the assessment of prestress loss over time, and the traction in the bars could be applied using hydraulic prestressing cylinders or torque wrenches (for low loads).

### *Model Experimentation*

Several tests were performed on the prestressed bridge prototype with four different types of load application. Then, when the SLT deck was loaded at more than one point, steel plates were used to uniformly distribute the applied weight in the points or areas of the model. After all the experiments had been concluded, the significant tests were: test 1 with a load at midspan of the deck as shown in Fig. 6(a); and test 2 with two loads applied at the longitudinal midspan and equidistant from the transversal edges of the plate according to Fig. 6(b).

**Table 1.** Two types of loading sequence used in test 1

| Type | Loading sequence (°) | Loads (kN) |
|---|---|---|
| 1 | 1 | 0 |
| | 2 | 3.3 |
| | 3 | 6.62 |
| | 4 | 9.93 |
| | 5 | 13.24 |
| | 6 | 16.54 |
| | 7 | 19.85 |
| | 8 | 23.16 |
| | 9 | 26.47 |
| | 10 | 29.78 |
| | 11 | 33 |
| 2 | 1 | 0 |
| | 2 | 4.96 |
| | 3 | 9.93 |
| | 4 | 14.89 |
| | 5 | 24.82 |
| | 6 | 29.78 |
| | 7 | 34.74 |
| | 8 | 39.71 |
| | 9 | 44.67 |
| | 10 | 46.96 |

Concerning the nondestructive tests, a sequence of loads according to Table 1 were applied at a rate of 2 kN/s. After reaching the first value of the sequence, the load was held for 60 s before the force had been reduced to 10% of that load level and was again maintained for 60 s, then the load was increased to the next load value of the required load sequence, and so on. A second cycle was applied to the plate so that the highest load level of that sequence could be reached and then completely removed from the plate.

The fifth experimentation represented the rupture test that was performed under the same conditions as the first test, in other words, with a concentrated load in the midspan of the deck.

Thus, for the rupture test of the deck, a load sequence was applied in the same way as the nondestructive tests, following the second loading type of Table 1 until the load of 46.96 kN be reached and kept for 60 s, then the load was reduced to 10% of that value and held for 60 s. After that, the load was then repeatedly increased by 3 kN each time up to the rupture.

Finally, the ultimate load was taken as that which corresponded to the beginning of the rupture of the most-loaded beam, which in this case was the central beam no. 14. Furthermore, although the ultimate load bearing capacity of the other beams that integrated the plate was not exceeded, the ultimate load value was equal to 105.9 kN.

### Analytical Model

The model was developed with the help of SAP90, in the SOLID module, which uses three-dimensional FEs and considers the orthotropic characteristic of materials. The first step was to fill the data entry with the material characteristics of the deck, so an initial attempt, typically intuitive, was to consider the deck as a solid wood board, where the MOE in the transverse direction (transversal to the longitudinal axis of the bridge) would have a value close to that found for a piece of wood or even higher if the contribution of prestressing was considered, but this hypothesis led to much smaller displacement values than those found in the experimentation. In other words, as was expected, the transverse stiffness of a SLT deck was completely distinct from a solid wood board of the same dimensions.

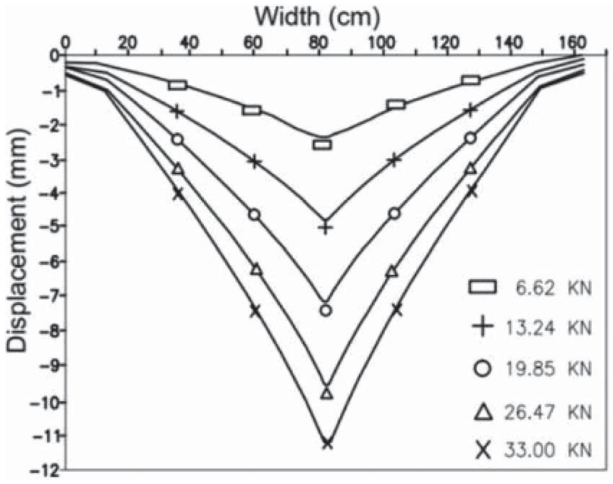


**Fig. 7.** Displacement profile in test 1 due to load type 1.

Then, looking for the best adjustment representing the behavior of an orthotropic plate using the FE program for the comparison of theoretical displacements with the experimental values allowed the simulation of many combinations until taking compatible values, thus the parameters of transverse stiffness and plate torsion had to be adjusted so that the theoretical and experimental profile of displacements could be similar.

Owing to the ease of setting up the data files, a plate of 2.40 m × 1.62 m × 11 cm was divided into 144 solid (three-dimensional) FEs of 8 nodes each, with a total of 338 nodes divided between the lower (169 nodes) and upper (169 nodes) surface of the plate. In addition, the apparent MOE values used in the numerical analysis were exactly those found in the tests performed according to the prior item that describes the bridge model.

### Deformation Analysis of Test 1 (Fig. 6a)

The LVDTs (D7–D13) distributed transversely to the longitudinal axis of the plate (third line) and positioned at the longitudinal midspan, as can be seen in Fig. 3, were used to obtain the highest arrow in that line as well as for the comparison of displacement profiles from numerical and experimental data as shown in Figs. 7, 8, and 9.

In addition, the LVDTs from lines at (1/4)*L* (D4, D5, D6, D14, D15, and D16) from the longitudinal edges (Fig. 3) were used for the comparison of experimental with theoretical deflections (D4 and D5). Thus, for the theoretical displacements, D4 and D5 (SAP90 FE analysis) were taken based on the theory that the others (D6, D14, and D16) should be the same value as D4 as well as when D5 is compared with D15, because of the "same" position of the LVDTs and the application point of the loading. In brief, for this reason only D4 and D5 (FE) appear representing the numerical analysis in Figs. 10, 11, and 12. In addition, in the first test setting we employed the two types of loading sequences as described in Table 1.

#### Deformations with First Loading Type

The displacement profile from the central line of the deck for the first loading type of test 1 is shown in Fig. 7, and the comparison between the displacements measured in the experiment by the LVDTs at (1/4)*L* of the plate edges (D4, D5, D6, D14, D15, and

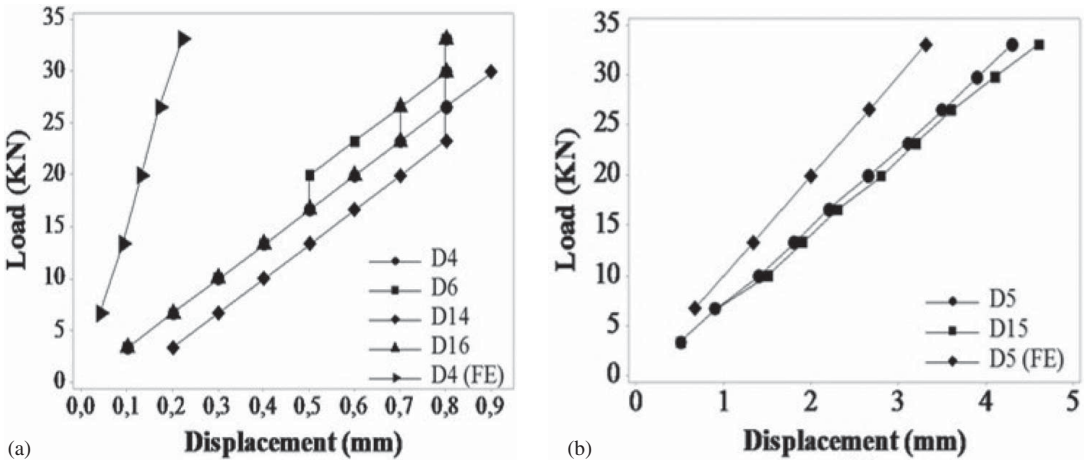


**Fig. 8.** Theoretical (FE) and experimental displacements at (1/4)*L* of the longitudinal edges of the plate: (a) lateral and (b) central border.

D16 in Fig. 3) versus the displacement values generated in SAP90 (FE) for D4 and D5 are shown in Fig. 10.

The largest displacement due to the first loading sequence of test 1 was 6.4 mm in D10 (Fig. 10a) with a load of 33 kN in the center of the plate, specifically in the midpoint of the load application, which was expected, because it is where the highest bending moment happened. The largest displacement in lines at (1/4)$L$ was 4.6 mm in D15 (load at 33 kN), which can be seen in Fig. 10(b) and is greater than the largest theoretical displacement (SAP90) of 3.31 mm in D5. However, when comparing the displacements from all LVDTs in the center line with the numerical ones, these values can be considered compatible owing to the similar displacement profile as much as the similarity of the inclination of the displacements according to the load level applied to the plate, especially in Fig. 10(b) for the (1/4)$L$ position.

### Deformations with Second Loading Type

Regarding the second loading sequence, the displacement profile from the center line of the plate for test 1 with LVDTs in the same position is shown in Fig. 8. Moreover, the comparison between the displacements measured in the experiment by the LVDTs at (1/4)$L$ of the plate edges (D4, D5, D6, D14, D15, and D16) versus the displacement values given by SAP90 (FE) in D4 as well as in D5 are shown in Fig. 11.

The largest displacement in the central line of the deck was 10.65 mm in D10 (Fig. 11a) with a load of 46.96 kN, which was the highest applied load in this sequence. The largest displacement in Fig. 11(b) that represents the displacements in the lines at (1/4)$L$ was 7.7 mm in D15 with a load of 46.96 kN, which is greater than the highest numerical value of 4.72 mm in D5 (FE) also contained in Fig. 11(b), but what can be seen in the graphs from Fig. 11 is a linear slope behavior with a certain proximity between experiment and numerical analysis especially as can be seen in Fig. 11(b) that represents the LVDTs from the midwidth of (1/4)$L$ of the deck.

### *Deformations Analysis of Test 2*

The displacement profile from the midlength of the plate for test 2 and the application of the second loading type is shown in Fig. 9. The displacement profile in Fig. 9 differs from the other two, because two equidistant loads were applied and positioned very close to the edges of the transversal side of the deck, which leads the laminates to be subjected to a greater shearing action and, at the same time, less flexion. In this case, the direction of the flexion is inverted as the points of application of the loads displace more than the midwidth part of the plate, thus being in agreement with the experimentation test.

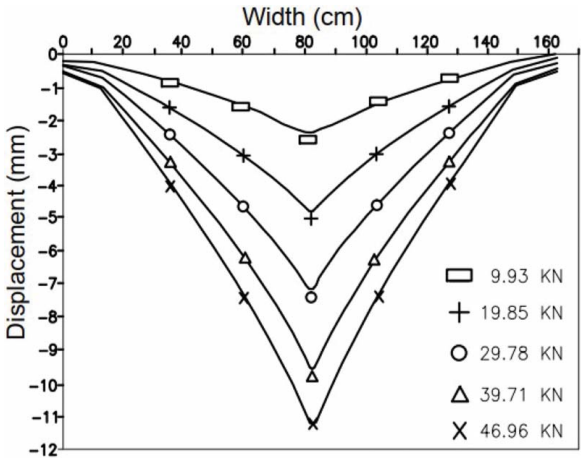


**Fig. 9.** Displacement profile in test 1 due to load type 2.

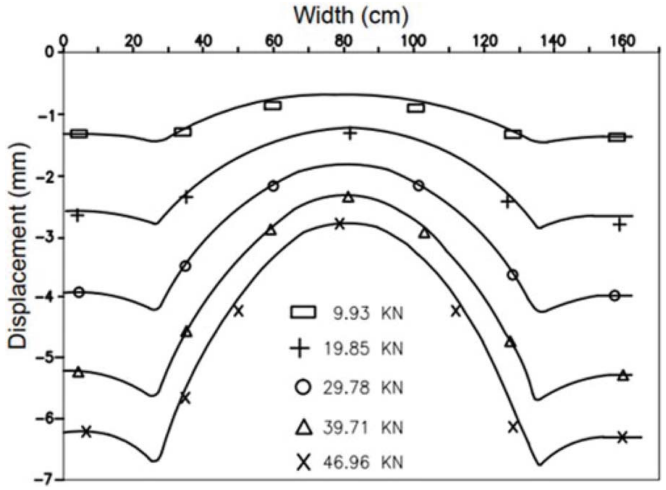


**Fig. 11.** Displacement profile in test 2 due to load type 2.

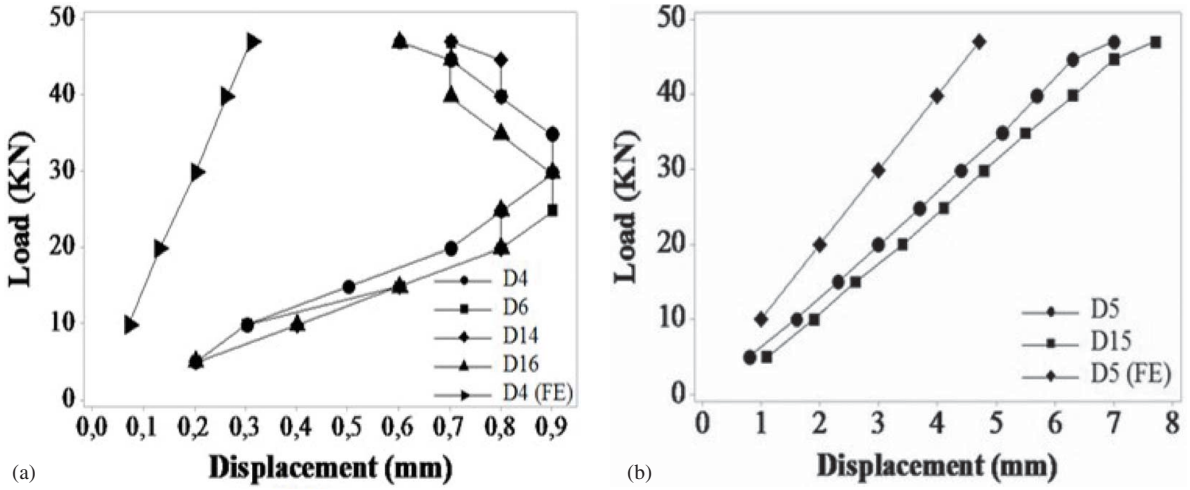


**Fig. 10.** Theoretical (FE) and experimental displacements at (1/4)$L$ of the longitudinal edges of the plate: (a) lateral and (b) central border.

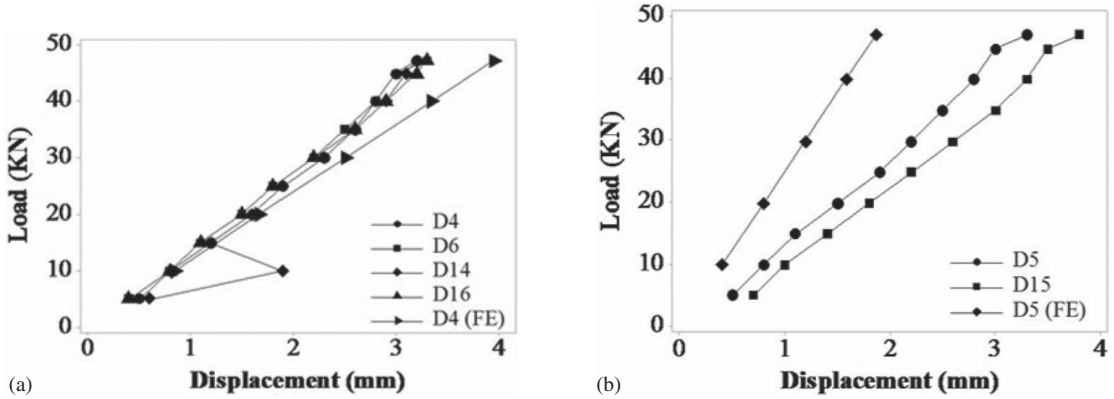


**Fig. 12.** Theoretical (FE) and experimental displacements at (1/4)$L$ of the longitudinal edges of the plate: (a) lateral and (b) central border.

The comparison between the displacements measured in the experiment by the LVDTs at (1/4)$L$ (D4, D5, D6, D14, D15, and D16) versus the displacement values by SAP90 (FE) in D4, as well as in D5 are shown in Fig. 12. The largest displacement found in this test at the midlength of the plate was 6.1 mm (Fig. 9) in D12 (Fig. 3), which is exactly one of the application points of loading, with a load of 46.96 kN (the highest of the sequence).

Furthermore, the largest displacement in Fig. 12, which represents the displacements in the lines at (1/4)$L$ from the longitudinal edges of the plate, was 3.8 mm in D15 (Fig. 12b) with a load of 46.96 kN, whereas the highest displacement in D5 (FE) was 1.87 mm also with a load of 46.96 kN. Although the calibration of the system is not very favorable, in Fig. 12(a) regarding the LVDTs of the lateral edges of the plate, it can be noted how the numerical and experimental analyses are practically identical in the displacement results as indicated by the similarity in the slope in Fig. 12(b) between the FE analysis and experimentation.

### *Analysis of Stress*

Experimental stresses were calculated using the linear ratio between stress and strain values

$$(\varepsilon) = [s](\sigma) \tag{1}$$

assuming the material has a linear, homogeneous, orthotropic, and elastic behavior.

For the case of an orthotropic plate in which directions of $x$ and $y$ axes coincide with the two principal directions of elasticity, according to Ribeiro (1986), Eq. (1) can be rewritten as matrix 1:

$$\begin{pmatrix} \varepsilon_x \\ \varepsilon_y \\ \gamma_{xy} \end{pmatrix} = \begin{vmatrix} S_{11} & S_{12} & 0 \\ S_{21} & S_{22} & 0 \\ 0 & 0 & S_{66} \end{vmatrix} \begin{pmatrix} \sigma_x \\ \sigma_y \\ \tau_{xy} \end{pmatrix} \tag{2}$$

Note that $S_{11} = 1/E_x$, $S_{22} = 1/E_y$, $S_{66} = 1/G_{xy}$, and $S_{12} = S_{21} = V_{xy}/E_x = V_{yx}/E_y$

The components of $(\sigma)$ are obtained by inverting $[S]$, according to matrix 2:

$$\begin{pmatrix} \sigma_x \\ \sigma_y \\ \gamma_{xy} \end{pmatrix} = \begin{vmatrix} C_{11} & C_{12} & 0 \\ C_{21} & C_{22} & 0 \\ 0 & 0 & C_{66} \end{vmatrix} \begin{pmatrix} \varepsilon_x \\ \varepsilon_y \\ \tau_{xy} \end{pmatrix} \tag{3}$$

where

$$C_{11} = \frac{E_x E_y}{E_y - E_x (V_{yz})^2} \tag{4}$$

$$C_{12} = \frac{E_x E_y V_{yz}}{E_y - E_x (V_{yz})^2} \tag{5}$$

$$C_{22} = \frac{E_x E_y}{E_x - E_y (V_{yz})^2} \tag{6}$$

$$G_{66} = G_{xy} \tag{7}$$

Therefore, the experimental normal stresses $\sigma_x$ and $\sigma_y$ were calculated through

$$\sigma_x = C_{11}\varepsilon_x + C_{12}\varepsilon_y \tag{8}$$

$$\sigma_y = C_{21}\varepsilon_x + C_{22}\varepsilon_y \tag{9}$$

where $\varepsilon_x$ and $\varepsilon_y$ are the experimental deformations measured by the electric strain gauges whereas the theoretical stresses were obtained through the FE nodes corresponding to the positions of the strain gauges. These stresses were measured at six points on each face (upper and lower) shown in Fig. 13, with two electric strain gauges at each point.

In general, the experimental stresses in regions near the anchor systems (points 1, 2, 3, and 4) were very close to or even higher than theoretical values in some cases. On the other hand, the experimental stresses at points 5 and 6 always presented values lower than those calculated by the FE method. In brief, these different behaviors between experimental and analytical stresses can be attributed to the effect of the prestress of the wood plate as well as by the different species used as laminates (beams).

Regarding the program chosen for calculation, it should be emphasized that theoretical values considered in the analysis are nodal tensions. Thus, the calculation of stress was initially performed at the midlength of the solid and FE so that the mean stresses at nodes can be calculated. In addition, the general steps taken from the assembly of the deck until the results were obtained are illustrated in Fig. 14.

## Discussion

The evaluation of prestressing forces applied to steel bars was missing an accurate analysis of the tensile stresses, because of problems with the electric strain gauge fixation, mainly as a result of the prestressing being performed manually. In this case, the installation of load cells could allow a good evaluation of the forces involved, providing the possibility of analyzing the prestressing losses over time, as performed by Ekholm et al. (2012) and Ekholm et al.

(2013). With the manual prestressing, it was possible to reach a load of 28 kN, whereas the required load was 30.8 kN, thus being lower than the minimum required by the Canadian standard. Nevertheless, the effect of this prestressing level was significant for the plate behavior.

The modest results of electric strain gauges attached to the bars and the manual prestress do not mean that this assembly is inefficient, but indicates that the nuts of the anchorage system have to be carefully tightened so that the region in which the extensometer has been glued is not affected. Obviously if DIWIDAG or RUDLOFF-VSL hydraulic prestressing cylinders are available, for example, the problems will certainly be reduced. For instance, in the study developed by Ekholm and Kliger (2014), a hydraulic jack was used for prestressing of bars. In addition, the anchorage system used (discrete plates) proved to be efficient in transferring stresses from steel bars to the wooden plate.

Regarding the two different types of loading, it was observed that a concentrated load in the center of the plate (first test) and two transverse concentrated loads in the middle of the longitudinal span of the deck (second test) are sufficient to have the transverse load distribution in the bridge model and the theoretical–experimental comparison. Moreover, by calculating the numerical (FE) displacements and stresses of the orthotropic plate, it was possible to evaluate an approximate transverse stiffness when applying the prestress, because the theoretical and experimental displacement profiles were quite compatible, which was also guaranteed owing to the linear elastic behavior during the tests (except the rupture test), being in agreement with the behavior found in Ekholm et al. (2012).

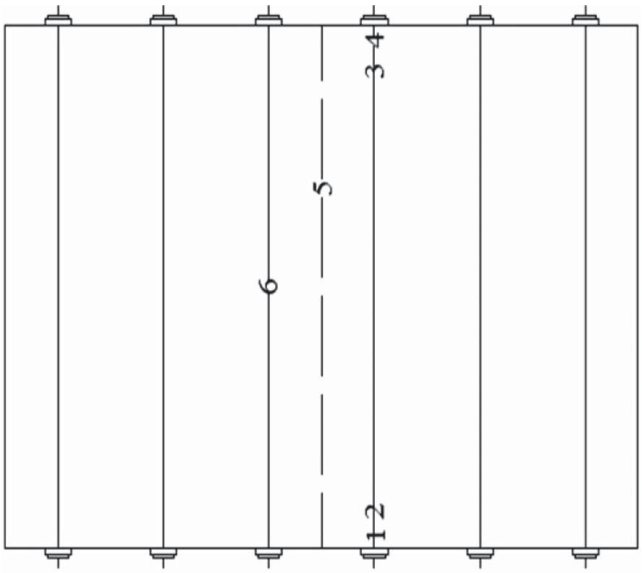


**Fig. 13.** Position of electric strain gauges for the reading of stresses.

The largest displacements always happened in the central line of the plate with the two sequences of loads within test 1 and also in the test 2 with the second loading type. To be specific, the highest displacement value in tests 1 and 2 were 10.65 mm at D10 and 6.1 mm at D12, respectively, then being consistent with the expectations, because these LVDTs were always in the point of load application.

Similarly, in lines at (1/4)$L$ from the longitudinal plate edges, the largest displacements were 7.7 mm at D15 and 4.6 mm also at D15 for the first and second sequence of loads in test 1, respectively. Concerning test 2, the highest value was 3.8 mm at D15. Although the results from test 2 at (1/4)$L$ are not in the point of load application, D15 was the only position in that line that was a considerable distance from the supports, then allowing this point to be the most affected between of the LVDT spots. In addition, almost all the experimental results of displacements were higher than numerical results, but very close to their relative values in Figs. 10, 11, and 12 calculated with SAP90, especially when it is observed that the displacement profiles were highly compatible between experimental and theoretical displacements.

A greater calibration of the numerical displacement results was not possible owing to the use of three species in the composition of the deck, which together plus the prestress made it very difficult to achieve an accurate precision, but, as the differences between the arrows were of the order of a few millimeters, these differences were not treated as a discrepancy. In fact, as can be seen in Fig. 10 that represents the results from test 1 with the second loading type, the numerical analysis resulted in higher displacement values for D5 and D15 (FE) at (1/4)$L$ from the longitudinal edges of the plate, which shows the effectiveness of the analysis.

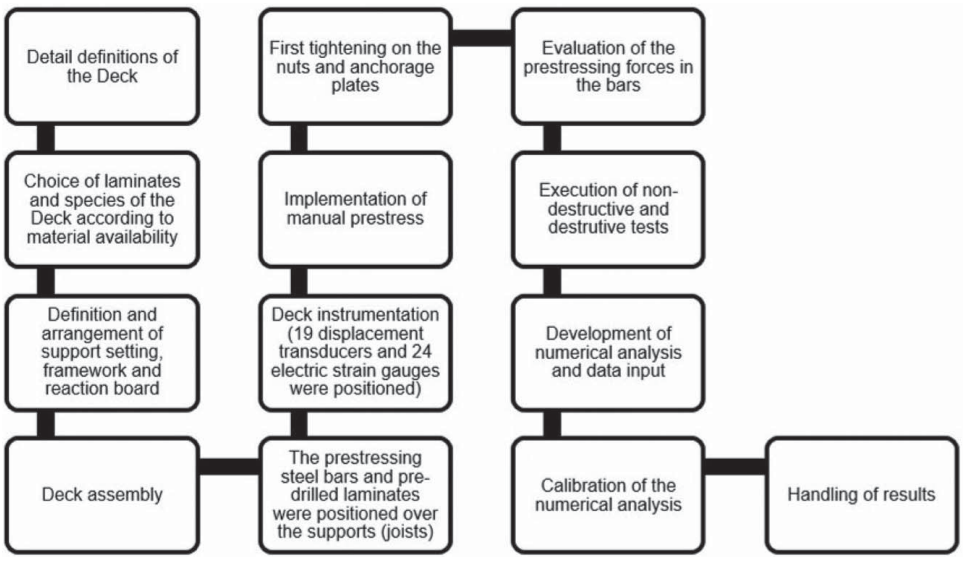


**Fig. 14.** Flowchart of the steps from assembly until the tests and results.

Furthermore, there was no interlaminar slippage when the plate was subjected to the first and second loading sequence for arrows lower than $L/400$, being in agreement with Ekholm and Kliger (2014). Concerning the parameters associated with transverse stiffness and torsion of the adopted plate in the numerical simulation, satisfactory results were achieved, showing the low transverse stiffness and reduced torsional strength of the considered orthotropic plate.

It is also important to register that the boundary conditions adopted in the numerical model (bifixed on edges parallel to the prestressing bars) were significant and closer to the behavior of the experiment owing to the adopted load types and the insignificance of the displacements over the supports. On the other hand, differences in wood anatomy constitution could lead to a different accuracy of the structural behavior of the deck as it indeed had an influence on the numerical model. In brief, a reasonable precision was found between the experiment and the analysis performed by SAP90.

## Conclusion

We can draw the following conclusions:

1. The deflections measured in the experimental tests were almost all lower than the deflections from the FE analysis in the software. However, in general, the results were very close and the displacement profile was similar to each other (experiment × FE method) and all the displacements were kept below $L/400$. Thereby, the results point to the fact that the theoretical analysis can predict the behavior of the SLT deck successfully.
2. The use of three different species of hardwood in the deck with the prestress applied to the bars made it difficult to obtain better system calibration, suggesting that a study in the future with just one species should be performed so that the optimal calibration of the numerical analysis could be reached.
3. No lateral slippage was observed for any nondestructive tests, indicating that the prestress and anchorage system (discrete plates) were effective when a SLT deck is constructed out of hardwood.
4. Initial expectations of orthotropic behavior for the plate were confirmed in this experiment, given the performance of the analyzed model. Therefore, the reasonable results prove the possibility of using hardwood species in this type of structure, which is in widespread use in the United States and Canada, but always built with laminates out of species from the conifer group.

## Data Availability Statement

All data, models, and code generated or used during the study appear in the published article.

## Acknowlegments

This study was financed in part by the Coordenação de Aperfeiçoamento de Pessoal de Nível Superior—Brasil (CAPES)—Finance Code 001.

## Disclaimer

The authors declare that they are responsible for all content including text, images, tables, and others.

## Notation

*The following symbols are used in this paper:*

$C_{11}$ = stiffness in the plane 1 and 1;
$C_{12}$ = stiffness in the plane 1 and 2;
$C_{21}$ = stiffness in the plane 2 and 1;
$C_{22}$ = stiffness in the plane 2 and 2;
$C_{66}$ = stiffness;
$E_x$ = modulus of elasticity in direction $x$;
$E_y$ = modulus of elasticity in direction $y$;
$F$ = force of prestressing load (kN);
$G_{xy}$ = shear modulus or transverse elastic modulus in the plane $x$ and $y$;
$G_{66}$ = shear modulus or transverse elastic modulus;
$L$ = length (m);
$S_{11}$ = flexibility in the plane 1 and 1;
$S_{12}$ = flexibility in the plane 1 and 2;
$S_{21}$ = flexibility in the plane 2 and 1;
$S_{22}$ = flexibility in the plane 2 and 2;
$S_{66}$ = flexibility;
$V_{yz}$ = coefficient of Poisson;
$X$ = bar reading ($\times 10^{-6}$ cm/cm);
$Y$ = load cell reading(N);
$\alpha$ = torsional parameter;
$\gamma_{xy}$ = vector of tension in the plane $x$ and $y$;
$\varepsilon$ = reduced vector of deformations;
$\varepsilon_x$ = vector of deformations in direction $x$;
$\varepsilon_y$ = vector of deformations in direction $y$;
$\theta$ = flexural parameter;
$\sigma$ = reduced vector of normal stress;
$\sigma_x$ = vector of normal stress in direction $y$;
$\sigma_y$ = vector of normal stress in direction $y$; and
$\tau_{xy}$ = vector of shear stress in the plane $x$ and $y$.

## References

Associação Brasileira de Normas Técnicas. 1997. *NBR 7190 – Projeto de estruturas de madeira*. Rio de Janeiro. 107.

Aydemir, D., A. Kiziltas, E. E. Kiziltas, D. J. Gardner, and G. Gunduz. 2015. "Heat treated wood–nylon 6 composites." *Composites, Part B* 68: 414–423. https://doi.org/10.1016/j.compositesb.2014.08.040.

Bakht, B., and L. Jaeger. 1985. *Bridge analysis simplified*. New York: McGraw-Hill.

Bakht, B., and L. Jaeger. 1992. "Simplified methods of bridge analysis for the third edition of OHBDC." *Can. J. Civ. Eng.* 19 (4): 551–559. https://doi.org/10.1139/l92-066.

Cavalheiro, R. S., D. H. Almeida, T. Almeida, A. Christoforo, and F. A. R. Lahr. 2018. "Estimation of modulus of elasticity in static bending of wood in structural dimensions as a function of longitudinal vibration and density." *Curr. J. Appl. Sci. Technol.* 26: 1–8. https://doi.org/10.9734/CJAST.

Crews, K. 2002. "Behaviour and critical limit states of transversely laminated timber cellular bridge decks." Ph.D. thesis, Faculty of Engineering, Univ. of Technology.

Crocetti, R., K. Ekholm, and R. Kliger. 2015. "Stress-laminated-timber decks: State of the arte and design based on Swedish practicey." *Eur. J. Wood Wood Prod.* 74 (3): 453–461. https://doi.org/10.1007/s00107-015-0966-1.

Davalos, J. F., S. S. Sonti, R. C. Moody, and R. Hernandez. 1996. "System stiffness for stress-laminated timber bridge decks." In *Proc., Int. Wood Engineering Conf.*, 213–220. Madison, WI: Omnipress.

Ekevad, M., P. Jacobsson, and G. Forsberg. 2011. "Slip between gluelaminated beams in stress-laminated timber bridges: Finite-element model and full-scale destructive test." *J. Bridge Eng.* 16 (2): 188–196. https://doi.org/10.1061/(ASCE)BE.1943-5592.0000153.

Ekholm, K., R. Crocetti, and I. R. Kliger. 2013. "Stress-laminated timber decks subjected to eccentric loads in the ultimate limit state."

*J. Bridge Eng.* 18 (5): 409–416. https://doi.org/10.1061/(ASCE)BE.1943-5592.0000375.
Ekholm, K., and I. R. Kliger. 2014. "Effect of vertical interlaminar shear slip and butt joints in narrow stress-laminated-timber bridge deck." *Eng. Struct.* 72: 161–170. https://doi.org/10.1016/j.engstruct.2014.03.023.
Ekholm, K., R. Kliger, and R. Crocetti. 2012. "Full-scale ultimate-load test of a stress-laminated-timber bridge deck." *J. Bridge Eng.* 17 (4): 691–699. https://doi.org/10.1061/(ASCE)BE.1943-5592.0000304.
European Committee for Standardization (CEN). 2004. "*Eurocode 5: Design of timber structures – Part 2: Bridges*." EN 1995-2, Brussels.
Figueroa, M., C. Bustos, P. Dechent, L. Reyes, A. Cloutier, and M. Giuliano. 2012. "Analysis of rheological and thermo-hygro-mechanical behaviour of stress-laminated timber bridge deck in variable environmental conditions." *Maderas-Cienc. Tecnol.* 14 (3): 303–319.
Karlsson, K., R. Crocetti, and R. Kliger. 2009. "Mechanical properties of stress-laminated timber decks—experimental study." In *Proc., 42nd CIB-W18*, 23–27. Gothenburg, Sweden: Chalmers Univ. of Technology.
Marques, L. E. M. M. 2008. "O papel da madeira na sustentabilidade da construção." M.S. thesis, Faculdade de Engenharia da Universidade do Porto.
Oliva, M. G., and A. G. Dimakis. 1988. "Behavior of stress-laminated timber highway bridge." *J. Struct. Eng.* 114 (8): 1850–1869. https://doi.org/10.1061/(ASCE)0733-9445(1988)114:8(1850).
Ribeiro, G. O. 1986. "Determinação de propriedades elásticas e de resistência dos compensados estruturais." M.S. thesis, Departamento de Engenharia de Estruturas, Escola de Engenharia de Sao Carlos, Universidade de Sao Paulo.
Ritter, M. A. 1990. *Timber bridges: Design, construction, inspection and maintenance*. Washington, DC: US Dept. of Agriculture, Forest Service.
Ritter, M. A., E. A. Geske, L. Mason, W. J. McCutcheon, R. C. Moody, and J. Wacker. 1990. "Performance of stress-laminated bridges." *Wood Des. Focus* 1 (3): 12–16.
Rodrigues, E. F. C., and A. L. Christoforo. 2019. "Evaluation of the potential use of Oiticica-Amarela wood for structural applications." *Int. J. Mater. Eng.* 9 (3): 23–27. https://doi.org/10.5923/j.ijme.20190902.01.
Schubert, S., D. Gsell, R. Steiger, and G. Feltrin. 2010. "Influence of asphalt pavement on damping ratio and resonance frequencies of timber bridges." *Eng. Struct.* 32: 3122–3129. https://doi.org/10.1016/j.engstruct.2010.05.031.
Segundinho, P. G. A., A. J. Regazzi, F. S. Poletti, M. O. Paula, A. R. Mendonça, and F. Gonçalves. 2018. "Variaç ao dos módulos de elasticidade e ruptura em madeira de cedro-australiano por meio de ensaios n ao destrutivo e destrutivo." *Ciênc. Florestal* 28 (3): 1163–1178. https://doi.org/10.5902/1980509833392.
Stavridis, L. T. 2001. "Alternative layout for the prestressing of slab bridges." *J. Bridge Eng.* 6 (5): 324. https://doi.org/10.1061/(ASCE)1084-0702(2001)6:5(324).
Taylor, R. J., and M. A. Ritter. 1990. "Developments in short and medium span bridge engineering '90." In Vol. 2 of *Proc., 3rd Int. Conf. on Short and Medium Span Bridges*, 391–402. Toronto, ON: Np.
Williamson, T. G. 1990. "Glued-laminated timber for bridge construction." *Wood Des. Focus* 1 (3): 4–6.